Statistical Analysis of Radar Rainfall Error Propagation

HATIM O. SHARIF

National Center for Atmospheric Research, Boulder, Colorado

FRED L. OGDEN

Department of Civil and Environmental Engineering, University of Connecticut, Storrs, Connecticut

WITOLD F. KRAJEWSKI

Department of Civil and Environmental Engineering, IIHR–Hydroscience and Engineering, University of Iowa, Iowa City, Iowa

MING XUE

School of Meteorology, and Center for Analysis and Prediction of Storms, University of Oklahoma, Norman, Oklahoma

(Manuscript received 7 March 2003, in final form 14 July 2003)

ABSTRACT

The prediction uncertainty of a hydrologic model is closely related to model formulation and the uncertainties in model parameters and inputs. Currently, the foremost challenges concern not only whether hydrologic model outputs match observations, but also whether or not model predictions are meaningful and useful in the contexts of land use and climate change. The latter is difficult to determine given that model inputs, such as rainfall, have errors and uncertainties that cannot be entirely eliminated. In this paper the physically based simulation methodology developed by Sharif et al. is used to expand this investigation of the propagation of radar rainfall estimation errors in hydrologic simulations. The methodology includes a physics-based mesoscale atmospheric model, a three-dimensional radar simulator, and a two-dimensional infiltration-excess hydrologic model. A time series of simulated three-dimensional precipitation fields over a large domain and a small study watershed are used, which allows development of a large set of rainfall events with different rainfall volumes and vertical reflectivity profiles. Simulation results reveal dominant range-dependent error sources, and frequent amplification of radar rainfall estimation errors in terms of predicted hydrograph characteristics. It is found that in the case of Hortonian runoff predictions, the variance of hydrograph prediction error due to radar rainfall errors decreases for all radar ranges as the event magnitude increases. However, errors in Hortonian runoff predictions increase significantly with range, particularly beyond about 80 km, where the reflectivity signal is increasingly dominated by three-dimensional rainfall heterogeneity with increasing range under otherwise ideal observing conditions.

1. Introduction

The scientific and technological advances of the past two decades have led to significant enhancements in forecasting of precipitation and in understanding and modeling of hydrologic processes. Construction of the Weather Surveillance Radar-1988 Doppler (WSR-88D) radar network and the deployment of a dual-polarization WSR-88D test bed are examples of headway that has been made in this field (Droegemeier et al. 2000). Many look to the national network of WSR-88Ds to provide the necessary information. Unfortunately, there is no unique relationship between precipitation rate and reflectivity measured by the radar. It is not unusual for radar-derived precipitation estimates to be in error by a factor of 2 or more. Because of earth curvature and atmospheric refraction the height of the radar beam above the earth's surface increases with range. Kitchen and Jackson (1993) asserted that the range effect is a major cause of underestimated rain accumulation. Furthermore, radar sampling volumes quadruple for every doubling of range. This resolution degradation increases the likelihood that precipitation fills only part of the beam and yields reduced reflectivity over that of a nearer volume.

In this study, we seek improved understanding of the sensitivity of a small infiltration-excess watershed to radar rainfall estimation errors with emphasis on the distance between the radar and catchment. Specifically, for a large number of simulated rainfall/runoff events, we seek to understand how the distance from the radar

Corresponding author address: Dr. Hatim O. Sharif, National Center for Atmospheric Research, P.O. Box 3000, Boulder, CO 80307.
E-mail: sharif@ucar.edu

to the watershed affects radar-estimated 1) catchment average rainfall volume, 2) peak discharge, 3) runoff volume, and 4) hydrograph root-mean-square error. These results have particular importance for predictions of flash flooding in small, infiltration-excess catchments, typical of urban and agricultural watersheds. The simulation framework includes simulated rainfall fields, assumed to be the ground ''truth,'' a radar simulator, and a physics-based distributed-parameter hydrologic model.

2. Simulation of radar rainfall estimation error propagation

The impact of radar rainfall estimation errors on hydrologic predictions from physics-based models is an important area of study, with broad applications ranging from flood forecasting to watershed ecology and management. Collier and Knowles (1986) found that, for a given percent error in the precipitation estimation, an equal or lesser error in the predicted streamflow would result for some catchments; but in other circumstances the errors were amplified. They suggested that underestimating rainfall could be worse than overestimation, especially for large catchments. Wyss et al. (1990) concluded that errors in runoff predictions caused by errors of radar-estimated precipitation were likely to be less significant than the errors in the transformation from rainfall to runoff. They suggested that identification of an appropriate reflectivity–rainfall relationship in real time is necessary to produce reliable hydrologic forecasts. Shah et al. (1996) asserted that the use of spatially distributed precipitation was far more important when modeling a dry catchment than when modeling a wet catchment. Using the System Hydrologique European (SHE) model on a 10.5 km^2 basin, they also concluded that errors associated with lumping of the model processes outweighed errors from lumping of the rainfall. Borga et al. (2000) found that radar rainfall biases magnify the rainfall/runoff transformation in humid mountainous watersheds. Winchell et al. (1997, 1998) found that error in radar rainfall estimates resulting from the use of inappropriate radar reflectivity–precipitation rate (Z–R) relationship resulted in equal or larger errors in predicted runoff, regardless of runoff production mechanism. Pessoa et al. (1993) showed that different widely accepted reflectivity–rainfall relationships resulted in significantly different hydrographs. Ogden and Julien (1994) identified two distinct sources of error when using radar rainfall inputs for hydrologic modeling, storm smearing, and watershed smearing. Storm smearing is caused by smoothing of rainfall-rate gradients in space with increasing radar pulse volume, and has the effect of changing the rainfall-rate distribution. Watershed smearing is caused by interactions between radar sampling volumes and watershed boundaries, which creates uncertainty about the location of rainfall with respect to the watershed.

Several researchers used physically based simulations of the radar measurement process to study the radar rainfall estimation error structure (e.g., Krajewski and Georgakakos 1985; Chandrasekar and Bringi 1987, 1988a,b; Chandrasekar et al. 1990; Krajewski et al. 1993; Anagnostou and Krajewski 1997; Borga et al. 1997). Krajewski et al. (1993) proposed a physically based simulator of radar observations based on a two-dimensional stochastic space–time model of rainfall events and a statistically generated drop-size distribution. Making several extensions to this simulator, Anagnostou and Krajewski (1997) complemented the two-dimensional fields with a vertical structure of hydrometeors by choosing a cloud-type model, which resulted in size, shape, and phase (mixed or single) distribution at discrete elevations. They simulated effects such as antenna beam pattern, horizontal and vertical gradients, atmospheric gases, and rain attenuation and represented the radar hardware noise by introducing random measurement errors. Borga et al. (1997) used the same tool to validate a brightband correction method.

Sharif et al. (2002) reported development of a simulation framework for the study of the impacts of radar rainfall estimation errors on hydrologic model predictions. The simulation framework is physically based and consists of an atmospheric model, a simulator of radar observations, and a distributed hydrologic model. Sharif et al. (2002) coupled a physically based atmospheric model of convective rainfall with an active microwave radiative transfer model to simulate radar observation of thunderstorms. Using the Advanced Regional Prediction System (ARPS) atmospheric model they simulated the well-documented tornadic supercell storm that occurred near Del City, Oklahoma on 20 May 1977 (Xue et al. 1995, 2000, 2001). Radar observations of that storm were then simulated and used to evaluate the effects of range and orientation between catchment and radar on distributed hydrologic simulations. In that study, Sharif et al. (2002) used a modified version of the radar simulator developed by Anagnostou and Krajewski (1997). The runoff was computed using the physically based distributed-parameter hydrologic model Cascade Two-Dimensional Model (CASC2D; Ogden and Julien 2002). This simulation framework allows examination of the impacts of radar rainfall estimation errors on land surface hydrologic predictions, while avoiding the limitations imposed by the use of rain gage data, such as undercatch, inadequate spatial sampling, point-area differences (Krajewski and Smith 2002), and gage calibration. Results from analysis of the 20 May 1977, supercell storm indicated that the geometry of the radar beam and coordinate transformations due to radar–watershed–storm orientation have an effect on both radar rainfall estimation and runoff prediction errors. In addition to uncertainty in the radar reflectivity versus rainfall intensity relation, Sharif et al. (2002) reported significant range-dependent and orientation-related radar rainfall estimation errors. Using that approach, the

authors were able to simulate several sources of radar measurement and estimation errors, both systematic and random and isolate the quantitative effects of various radar-related sources of uncertainty. Pulse volume and beam height were found to be the most dominant source of errors at ranges greater than 50 km, much more significant than the influence of random errors such as raindrop-size distribution variation and radar noise.

3. Objectives

In this present study, a storm that covers a large area is simulated, allowing the location of the study watershed to be moved within the storm domain and the generation of different realizations of the rainfall–radar–runoff transformation process. This allows us to significantly expand on the approach demonstrated in Sharif et al. (2002), and develop meaningful statistics based on a much larger number of simulations. Inherent in the investigation is the assumption that the rainfall generated by the atmospheric model, which is a realistic representation of convective storm, is the ground truth. A radar simulator is run and radar-estimated rainfall is used from the simulated storm as input to a physically based, infiltration-excess, hydrologic model. Our fundamental objective is to analyze the propagation of radar rainfall estimation errors through runoff predictions with emphasis on the range effect. The spatial and temporal structure of the precipitation domain, combined with use of 500 watershed locations within the storm domain, allow the development of an ensemble of rainfall/runoff events with different rainfall fields. The ensemble is large enough to produce adequate statistics of the range dependence of radar-estimated rainfall errors and the propagation of these errors in runoff predictions for watersheds of this shape and size. Statistics of the influence of radar range on rainfall and runoff errors are computed. Relationships between rainfall volume, runoff volume, and peak discharge errors and their range-dependence are statistically analyzed. Because from our previous study, Sharif et al. (2002), we found that range errors are orientation-dependent, we average error statistics for each radar range over 24 orientations. In addition to the influence of radar range, the relationship between the rainfall event magnitude and the prediction error is also examined. The results of the present study are more general than the results shown in the demonstration of the methodology by Sharif et al. (2002), because the morphology of the widespread convective rainstorms used in this present study is much more varied.

4. Storm simulation

The source of precipitation fields used in this study is the ARPS simulation performed at 500-m horizontal resolution and vertical resolution ranging from 20 m near the ground to nearly 1 km at the model top, for the 21–22 January 1999 tornado outbreak that severely impacted the U.S. state of Arkansas. The ARPS is a three-dimensional, nonhydrostatic compressible atmospheric model formulated in generalized terrain-following coordinates. It contains a comprehensive physics package and a self-contained data analysis, radar data retrieval and assimilation system. The model has been subjected to real-time weather prediction testing over several regions since the mid-1990s. A comprehensive description of the formulation, numerical solution methods, physics parameterizations, computational implementation, and configuration instructions for the ARPS is given in Xue et al. (1995). More recent improvements and model verifications are described in Xue et al. (2000, 2001, 2003).

During the afternoon and evening of 21 January 1999, a sequence of thunderstorms occurred along the southwest–northeast diagonal axis of the state of Arkansas (AR). Many of these storms, which produced significant amounts of precipitation, contained strong vertical motion. A total of 56 tornadoes were reported statewide with the strongest tornadoes rated F3 (maximum winds 71 to 92 m s^{-1}) on the Fujita scale. Most of the tornadoes, which unfortunately caused eight deaths, occurred between 0400 and 2300 central standard time (CST), or between 2200 UTC 21 January and 0500 UTC 22 January. This event is believed to be the largest tornado outbreak in Arkansas up to this date.

The synoptic-scale features and events of this case were documented in Xue et al. (2001), together with the ARPS model prediction results on nested 32- and 6-km resolution grids. For all simulations, fourth-order advection and computational mixing were used. The physics options include the 1.5-order turbulent kinetic energy (TKE)-based subgrid-scale turbulence and planetary boundary layer (PBL) parameterization, a two-layer soil model, explicit grid-scale ice microphysics and National Aeronautics and Space Administration Goddard Space Flight Center (NASA GSFC) radiation physics. Cumulus parameterization scheme was used only on the coarsest 32-km grid. With the ice microphysics scheme, ARPS explicitly predicts five water and ice categories, namely, cloud water and cloud ice, rainwater, snow, and hail (Lin et al. 1983; Tao et al. 1989). References for other physics options can be found in Xue et al. (2000, 2001, 2003).

Both 32- and 6-km grids successfully predicted the general precipitation area aligned along the southwest–northeast diagonal of the state of Arkansas. The onset of precipitation using ARPS with a 6-km grid was delayed by as much as 4 h. Prediction results were much improved when a 2-km grid was further nested within the 6-km grid. The 2-km results were analyzed and compared with radar observations in Xue et al. (2003). These forecasts started at 1200 UTC on 21 January, 8 h prior to the first convective storms (about 2000 UTC) in Arkansas, and about 10 h before the first tornado (2200 UTC). For a 10-h period beginning 8 h into the ARPS

run (2000 UTC), there is general agreement with respect to the number of storms in the state of Arkansas, the rotational characteristics of these storms, and the speed and direction of storm-cell movement. There is additional consensus with respect to the organization of initially isolated cells into lines and their subsequent propagation, the transition from a straight line into a mesoscale bow-shaped echo pattern, and the reasonable timing of thunderstorm initiation and cessation of new cell development.

Specifically, at 2300 UTC 21 January about a dozen storm cells can be identified both in radar observations and in the model, and both model and real storms exhibit isolated supercell storm characteristics with rotation more readily identifiable in the model (see Xue et al. 2003). For the next 3 h, from 2300 UTC 21 January to 0200 UTC 22 January, both observations and model simulations showed new cells continually being generated at the south end of the convective line while older cells moved along the diagonal axis across the state of Arkansas. By the end of this 3-h period, the line in the model has turned more into the SW–NE orientation. As more cells were created through the splitting process and as the low-level cold pool spread, the storms became closer to each other. As a result, some joined together, creating connected line segments.

In the 2 h following 0200 UTC, the trend for the cells to merge and form a continuous line continued both in the model and in the real world. By 0400 UTC, the southern end of the primary line is shown two to three counties away from the southern state border. At 0600 UTC 22 January, the end time for the 2-km simulation, the convective line was moving (eastward) across the eastern Arkansas state border.

The focus of this paper is the period between 0200 and 0430 UTC 22 January, when the initial supercell storms evolved into the precipitation line, located in the northeastern region of Arkansas and southeast Missouri. The finescale features and spatial variabilities of precipitation were studied. In this study, a simulation with an even higher 500-m-resolution grid covering a 128 km $\times$ 128 km region of precipitation is performed at a 2-s time step to capture additional finescale details. This grid is nested inside the 2-km domain. Instantaneous model-predicted precipitation rates from this 500-m simulation are plotted in Fig. 1 at 30-min intervals.

5. Radar estimation process simulation

The radar simulator extracts three-dimensional values of pressure, temperature, rainwater content, and water vapor content from ARPS output to compute gradients of atmospheric refraction. We simulate radar beam propagation in three-dimensional space with consideration of the beam curvature relative to the earth's curvature. The three-dimensional fields of rainwater computed by ARPS are used to compute the volume backscattering and extinction cross sections of hydrometeors (Ulaby et al. 1981). Although the radar simulator calculates the refractive index at each grid cell, a constant value of the refractive index slope was used because of the relatively small impact on the hydrologic model output (Sharif et al. 2002). The radar simulator also includes dual-polarization capability, but we did not use this feature. Our study was confined to single-polarization radar hardware, and used the default WSR-88D Z–R relationship of $Z = 300R^{14}$ (Fulton et al. 1998) to convert reflectivities into rainfall-rate estimates. The radar wavelength is assumed to be 10 cm, the beam elevation angle is 0.5°, and the half-power beam width is 1°, close to WSR-88D's value of 0.95°. The azimuthal resolution of radar observations is 1°. The attenuation of electromagnetic waves by rain was computed from the radar as a function of the radar wavelength (10 cm), rainfall intensity, and distance between radar and hydrometeors. Attenuation by atmospheric gases, which is typically larger than rain attenuation for S band, is only a function of radar wavelength and distance (Doviak and Zrnic 1993). Because the attenuation of atmospheric gases can be accounted for in real radar data processing systems, it is not modeled in this study. The ability of the radar simulator to produce radar reflectivity fields similar to those estimated by ''true'' radars was demonstrated in previous applications, e.g., Anagnostou and Krajewski (1997) and Borga et al. (1997).

The hydrologic model CASC2D was run using the true ARPS-generated rainfall fields and radar-estimated rainfall fields. Hydrologic model outputs were compared based on the true rainfall and the radar-estimates-based rainfall by calculating four error statistics. These statistics are: the watershed total rainfall volume ratio, the root-mean-square error in simulated hydrograph, the simulated total runoff volume ratio, and the hydrograph peak discharge ratio.

The main simulations focus on the effect of range and highlight the spatial variability of the vertical rainwater (or reflectivity) profile within the same storm as well as to feature its impact on hydrologic model predictions. Although the atmospheric model included ice microphysics in its simulations, radar simulations above the freezing level were not conducted.

6. Radar–storm–watershed setting

The watershed simulated in this study is the 21.2 km^2 Goodwin Creek experimental watershed located in north-central Mississippi. The U.S. Department of Agriculture–Agricultural Research Service (USDA–ARS) National Sedimentation Laboratory has continuously monitored the watershed since 1981. Alonso (1996) provides a detailed description of the watershed. The elevation of the watershed ranges from 68 to 127 m and the main channel has an average slope of 0.004 (Bingner 1996). The grid size used in CASC2D to model the watershed is 125 m $\times$ 125 m, a compromise between computational time and adequate description of the spa-

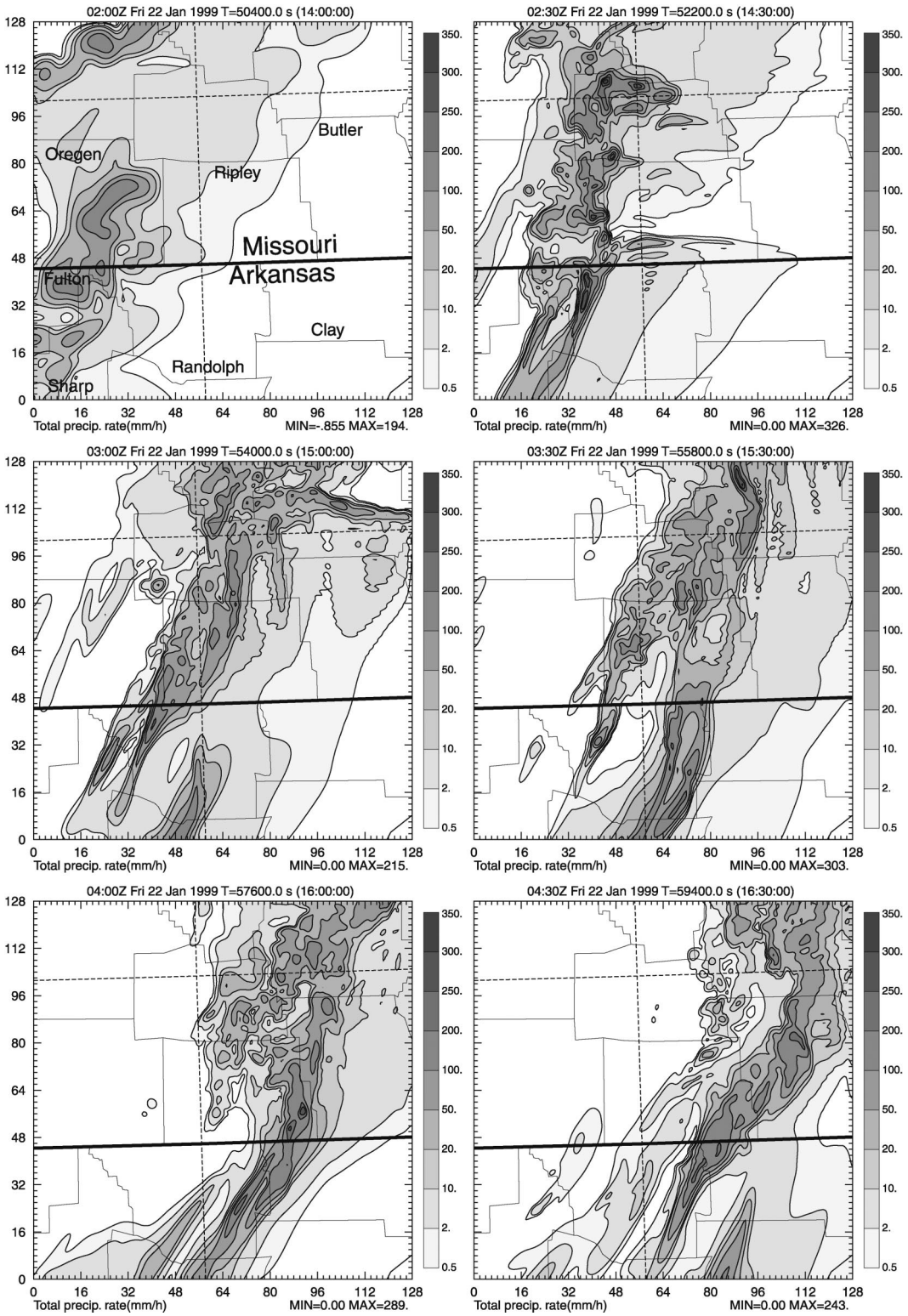

FIG. 1. Instantaneous rain rates (mm h^{-1}) from the ARPS-simulated 21–22 Jan 1999 Arkansas tornado outbreak case. The plots correspond to the period between 0200 UTC and 0430 UTC 22 Jan at 30-min intervals. Missouri and Arkansas border marked by the thick line, and most counties labeled at top left.

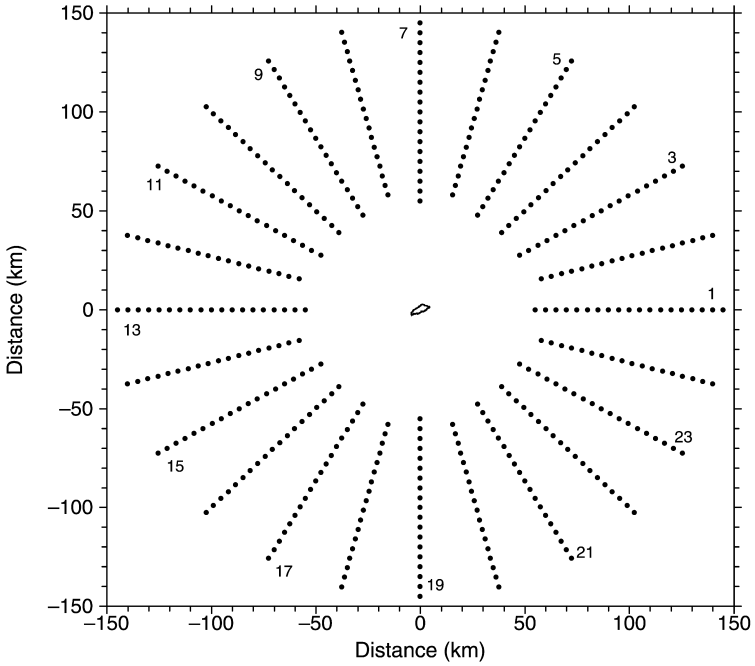

FIG. 2. Configuration of the simulated radar orientations around Goodwin Creek. The radar range is varied along these orientations from 10- to 145-km in 5-km increments.

tial variability of topography, soil texture, and land use/land cover. The watershed characteristics, taken together with the predominance of fine soil textures, indicate that the Hortonian runoff production mechanism is dominant during the growing season (Senarath et al. 2000; Ogden and Dawdy 2003). The hydrologic model CASC2D was rigorously calibrated and verified on this watershed by Senarath et al. (2000), who found the model to produce unbiased predictions of runoff response. Downer and Ogden (2003) showed that the model represents the watershed's runoff processes with reasonable accuracy by verifying model predictions of soil moisture profiles at two locations in the catchment. The watershed is approximately 9.5 km in length, and 4 km in maximum width. Watersheds of this size can be severely impacted by convective rainfall, with high likelihood for loss of life due to flash flooding (Ogden et al. 2000). The initial soil moisture state can have a significant effect, but only if the soils are extremely wet or dry (Ogden and Dawdy 2003). We used a constant, intermediate value of initial soil moisture to minimize this effect on our results.

We account for the influence of radar–watershed orientation by placing the radar at 24 equispaced orientations (every 15°) and vary the range along these directions, as shown in Fig. 2, and then take the average value from these 24 orientations. The distance between the radar and the center of the catchment is varied along these directions from 10 to 145 km in 5-km range increments. We limited the range to 145 km to keep the beam below the freezing level. The 28 range increments were the same for all 24 radar orientations in all watershed locations. The orientations were coded with numbers 1–24, orientation 1 being exactly east of the watershed center. True rainfall fields were directly input to the hydrologic model on a 500 m × 500 m grid, with each ARPS grid cell containing exactly 16 CASC2D model grids. Radar rainfall estimates were input to the hydrologic model in polar coordinates using the ''nearest neighbor'' method to assign rainfall rates from pulse volumes to each hydrologic model grid. The radar simulator was run using a 5-min time step.

The purpose of the majority of the simulations is to develop a large sample of rainfall/runoff events in which the radar rainfall errors are only caused by the effects of range between the radar and the study watershed. Because of the high variability of rainfall within the mesoscale convective complex, the watershed was placed in 500 different locations within the 128 km × 128 km storm domain as a means to obtain different cases of the radar estimation process. Justification for this radar–storm–watershed setting can be found in Sharif et al. (2002).

Comparison error statistics were computed after each hydrologic model simulation. The rainfall volume error measure, ε_m, is the ratio between radar-estimated catchment total rainfall (rn^{est}) volume and the reference total rainfall volume at the ground level (rn^{ref}) computed by ARPS model:

$$\varepsilon_{rn} = \frac{rn^{est}}{rn^{ref}}. \quad (1)$$

The measures of the influence of radar error on hydrologic model response are three of the statistics typically used to calibrate hydrologic models and evaluate their performance (e.g., Brazil 1988). Root-mean-square error percentage (rmse%) is computed using

$$\text{rmse\%} = \frac{100}{\text{pk}^{\text{ref}}}\sqrt{\frac{1}{N}\sum_{i=1}^{N}(q_i^{\text{est}} - q_i^{\text{ref}})^2}\%, \qquad (2)$$

where q^{est} is the simulated discharge driven by radar-estimated rainfall and q^{ref} is the corresponding discharge ordinate resulting from the reference ARPS-modeled rainfall, that is, the hydrograph produced using ARPS rainfall fields is assumed to be the reference hydrograph. The value N refers to the total number of hydrograph ordinates used in the analysis, while i is the index denoting individual hydrograph ordinates. Here, N is usually in the order of 1500 points; pk^{ref} is the reference peak discharge.

The error in the peak discharge, ε_{pk}, is expressed as the ratio between the estimated peak discharge using radar rainfall (pk^{est}) and the reference peak discharge (pk^{ref}):

$$\varepsilon_{\text{pk}} = \frac{\text{pk}^{\text{est}}}{\text{pk}^{\text{ref}}}. \qquad (3)$$

The error in runoff volume, ε_{ro}, is similarly expressed as the ratio of the estimated (ro^{est}) and reference total runoff volumes (ro^{ref}):

$$\varepsilon_{\text{ro}} = \frac{\text{ro}^{\text{est}}}{\text{ro}^{\text{ref}}}. \qquad (4)$$

7. Results and discussion

We computed rainfall and hydrograph error measures for all 500 rainfall/runoff events. For each radar range we computed errors for 24 radar orientations; a total of 12 000 values for each radar range. As found by Sharif et al. (2002), errors generally increase with radar range, and errors in runoff volume and peak discharge are typically larger than the corresponding errors in rainfall volume. Plots of probability density function (pdf) for the four error measures are shown in Fig. 3. We compare pdf histograms for two radar ranges, 100 and 145 km from the watershed center. Taking into account that all histograms in Fig. 3 consist of 20 classes, and that small values on the edges of the histogram may not be visible in the plot will make it easier to compare different histograms.

Rainfall volume ratio pdf histograms, Figs. 3a,b, appear approximately Gaussian and peak near the value of 1.0 for both radar ranges. The range of storm total accumulated rainfall error values is relatively small, between 0.88 and 1.08 for the 100-km radar range, and increases to 0.78 to 1.24 for the 145-km radar range. For both radar ranges, there is slightly greater tendency towards underestimation than overestimation. The 145-km radar range pdf curve, shown in Fig. 3b, is more flat—indicating higher standard deviation. The standard deviation is plotted as a function of radar range in Fig. 4a. The dependence on range is very obvious for ranges beyond 100 km.

It is clear from Fig. 3c that rainfall errors are significantly amplified in predicted runoff although rainfall and runoff error pdfs do not seem significantly different. The runoff volume error pdf histogram is more flat and has a significantly larger range than the rainfall volume error pdf histogram, an indicator of the sizeable difference in variance of the two distributions. This can be seen by comparing Figs. 3a and 3c. The distributions of the rainfall, runoff, and peak discharge errors are approximately Gaussian whereas the RMSE distribution is nearly lognormal. Comparing the two histograms of Figs. 3c and 3d, reveals that runoff volume error variance increases with range—the 145-km radar range histogram is more flat with a wider range on both cases of underestimation and overestimation. The range dependence of rainfall volume and runoff volume errors is quantified in Figs. 4a,b.

For all radar ranges, the error in hydrograph peak discharge is more pronounced than runoff volume error. The peak discharge error pdf plot is similar to the runoff volume error plot except for a slight difference in flatness and a wider range of values. Figures 3e,f show that the range of peak discharge error values for the 145-km radar range is more than twice the range of error values for the 100-km range, and that the pdf curve is more flat. Like the runoff error pdf, the peak discharge pdf shows a slight tendency towards underestimation. The increase of standard deviation with range is demonstrated in Fig. 4c.

As expected, the pdf histogram of the hydrograph RMSE percentage is skewed towards smaller values. This is because RMSE percentage distribution is related to the distributions of runoff volume and peak discharge errors; both distributions peak near the value of 1.0. Figures 3g,h show that RMSE percentage increases with radar range and the tail of the 145-km radar range pdf histogram is considerably more extended than that of the 100-km radar range histogram. The variance of RMSE percentage strongly depends on range for ranges beyond 100 km and the increase of the standard deviation with range is sharp and almost linear for ranges farther than 115 km, as shown in Fig. 4d.

The standard deviations of the rainfall volume error, Fig. 4a, runoff volume error, Fig. 4b, peak discharge error, Fig. 4c, and RMSE error, Fig. 4d, show little dependence on range for radar ranges less than 90 km. The increase in standard deviation is very sharp for ranges beyond 90–100 km for Figs. 4a–d. The slope of the curves in Figs. 4a–d is almost constant for ranges beyond 110–120 km, indicating a linear increase in standard deviation with range.

Errors in rainfall volume are amplified in the transformation to predicted runoff for all 28 radar ranges

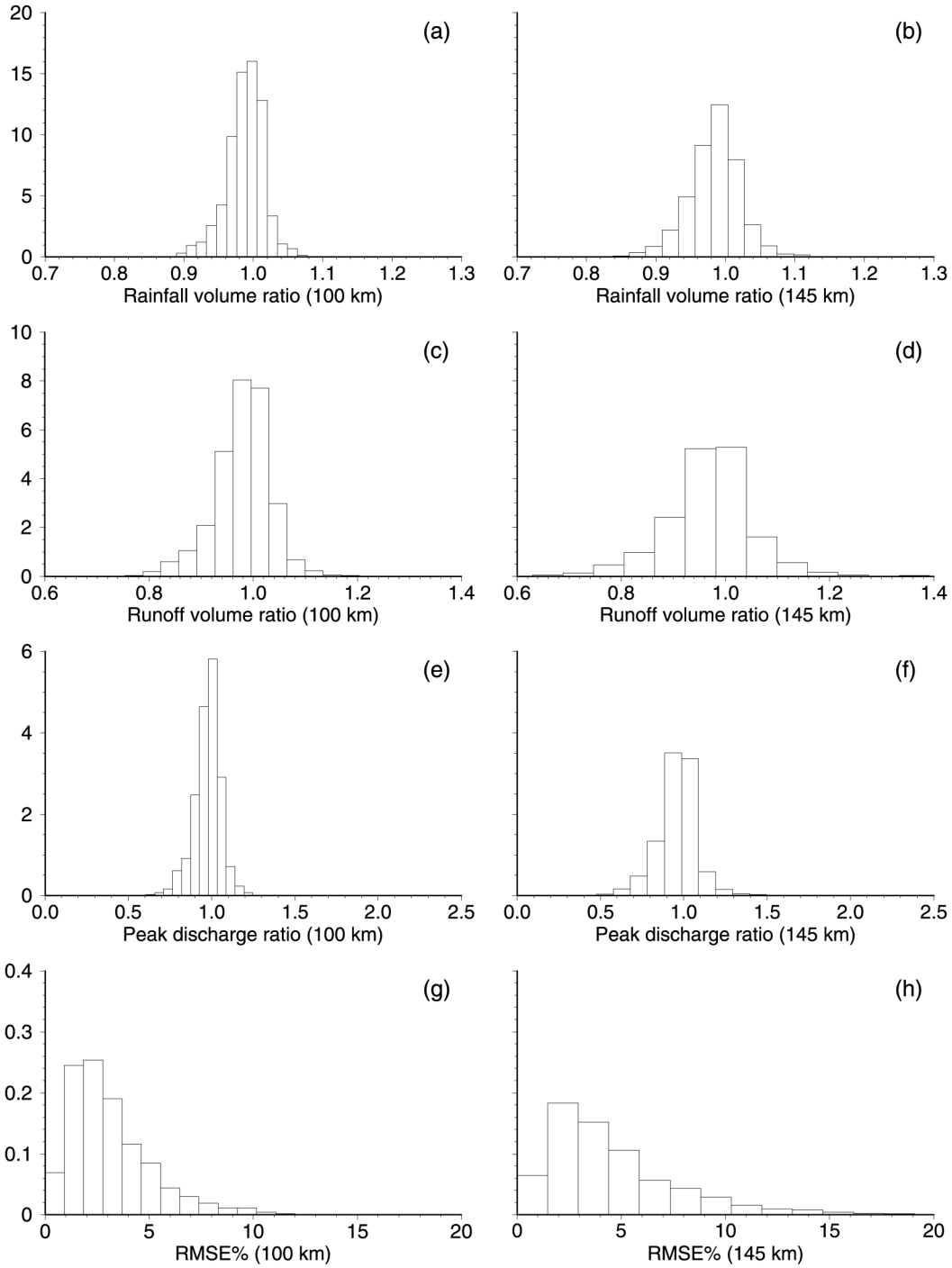

FIG. 3. Probability density functions of radar-estimated (a) rainfall volume, (c) runoff volume, (e) peak discharge ratios, and (g) RMSE% for the radar range of 100 km. (b), (d), (f), (h) The same as in left column except for radar range of 145 km.

considered. For example, the amplification of error can be seen in Figs. 5a,b for two radar ranges. The plot of peak discharge error versus runoff volume error shows increased underestimation and overestimation in peak discharge as compared to runoff volume. This is indicated in Figs. 5c,d. When the errors are very small, that is, close to the value of 1 in both axes, the scatter of points is less, and points are almost evenly distributed around the 1 to 1 line. This is the case for both radar ranges.

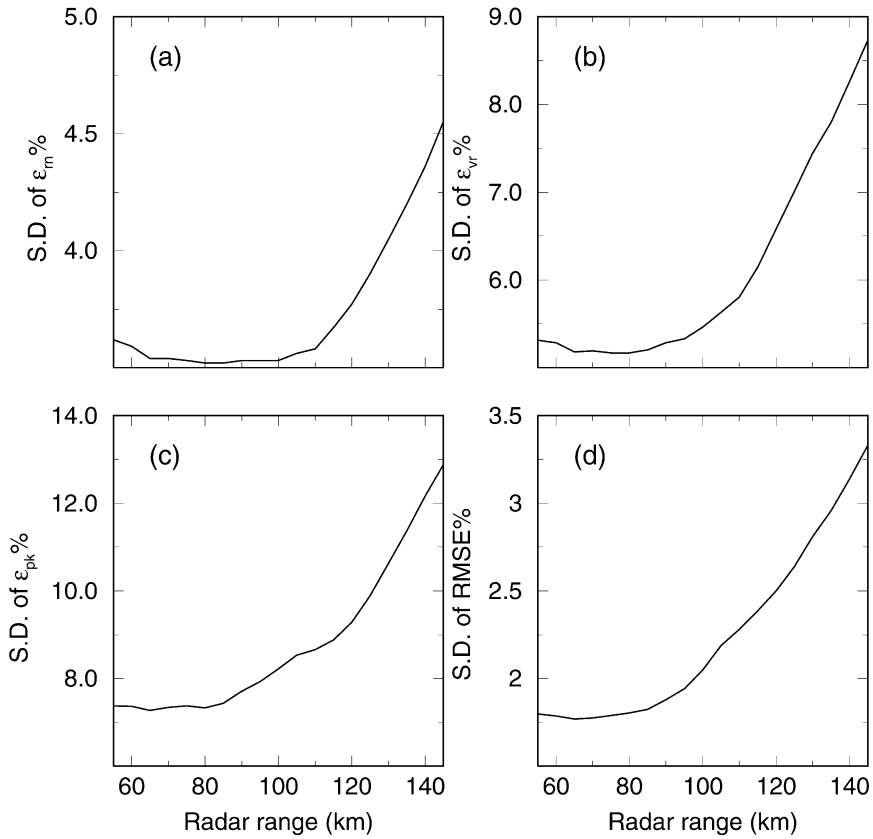

FIG. 4. Range dependence of the standard deviation of (a) rainfall volume, (b) runoff volume, (c) peak discharge, and (d) RMSE% errors.

To check whether the relationship between rainfall volume, runoff volume, and peak discharge errors is range-dependent, regression analysis was performed to compute the relationship between these errors at different ranges. When runoff volume error (ε_{ro}) is plotted against rainfall volume error (ε_{rn}), the slope of the regression line will always be greater than 1, as shown in Fig. 5. The slope of the regression line is plotted as a function of range in Fig. 6a. Figures 6a,b confirm that amplification of radar rainfall error increases with radar range as measured by the corresponding runoff volume or peak discharge errors. The relationship between peak discharge and runoff volume errors, (ε_{pk}) and (ε_{ro}), does not depend on radar range or the magnitude of the rainfall error. This is evident from Fig. 6c or when comparing Figs. 5c and 5d. It can be understood that the rainfall error increases with range both in terms of magnitude and corruption of the spatial structure of the rainfall field, which will lead to increased amplification of errors in the predicted runoff. The watershed response is scale-dependent (Giannoni et al. 2003) and the relationship between peak discharge and runoff volume is more complex and highly nonlinear because of dependence of peak discharge on the rainfall rate at the Goodwin Creek Experimental Watershed (Ogden and Dawdy 2003). However, the ratio of the slope of runoff error versus rainfall error to the slope of peak discharge error versus runoff error, Fig. 6d, is basically constant except for the ranges where the curve in Fig. 6c shows this sudden decrease.

The fact that the predicted runoff volume error (ε_{ro}) is larger than the rainfall volume error (ε_{rn}) and that peak discharge error (ε_{pk}) is typically larger than runoff volume error (ε_{ro}) is expressed in probability format in Fig. 7. For each rainfall volume error value, the magnitude of the corresponding error in runoff volume is used to identify it as amplification or damping of the error. This information was used to construct the probability distribution of error amplification shown in Figs. 7a,b. The same was done to construct Figs. 7c,d based on runoff volume and peak discharge errors. For the 100-km radar range in Fig. 6a and both radar ranges in Figs. 7c,d, it can be seen that the maximum value of the probability is close to 0.5. This occurs when there are very small errors in rainfall volume, as seen in Fig. 6a, or with runoff volume, as seen in Figs. 7c,d. It has to be stressed that it is possible that the ratio of the radar-estimated and true total rainfall volume can be close to 1.0 and yet the radar and actual rainfall fields will not be identical. For the 145-km radar range, as seen in Fig. 7b, it was found that when the error in rainfall volume is very small, the runoff volume error

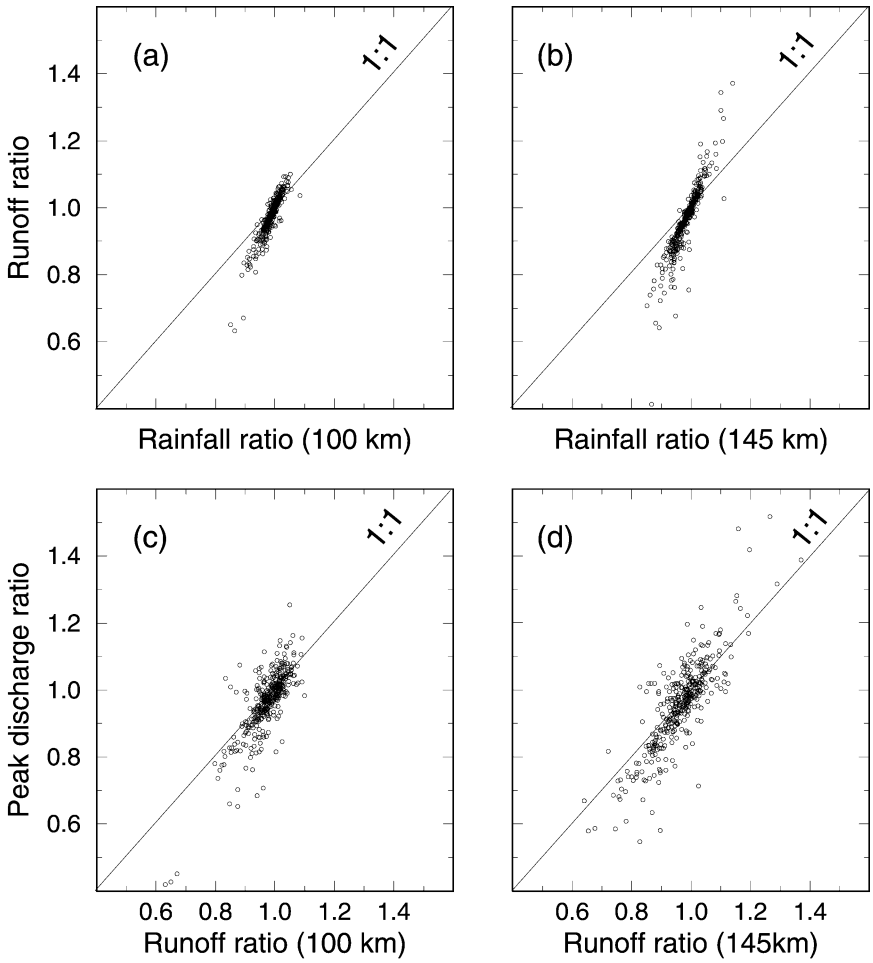

FIG. 5. Relationship between (a) radar-estimated rainfall volume error (ε_{rn}) and runoff volume error (ε_{ro}), and between (c) runoff volume error (ε_{ro}) and peak discharge error (ε_{pk}), for the radar range of 100 km. (b), (d) The same as in left column except for radar range of 145 km. The errors shown are for one of the radar orientations using results from all 500 watershed locations tested.

is less than rainfall volume error in less than 25% of the cases. A detailed discussion on the existence of significant runoff volume errors, even when radar and actual rainfall volumes are equal, can be found in Sharif et al. (2002). The spikes on the sides of the probability plots occur when the concentration of points is very sparse as seen in Fig. 5.

An important factor that influences the magnitude of error in radar-estimated rainfall volume and, more importantly, its propagation through hydrograph predictions is the magnitude of the rainfall/runoff event. The value of radar-estimated rainfall volume and actual rainfall volume ratio is plotted against the actual rainfall volume in Fig. 8a, which demonstrates that rainfall volume errors are generally larger for small rainfall events. The scale of the plot conceals some of the dependence on the magnitude of the rainfall event, however, the relationship is not very strong. This relationship between event and error magnitudes also holds for the runoff volume error, Fig. 8b, peak discharge error, Fig. 8c, and RMSE error, Fig. 8d. All plots in Fig. 8 show the average error from all 24 orientations for the radar range of 145 km. Plots for other radar ranges show similar trends. The plots are similar when we plot the maximum or minimum error value of the 24 orientations against the event magnitude for all radar ranges.

8. Summary and conclusions

This study presents results of a large number of hydrologic simulations driven by physically realistic radar rainfall estimates. We use an observing system simulation framework for investigating the propagation of radar rainfall estimation errors in runoff predictions. A state-of-the-art atmospheric model is used to simulate a storm that covers a large (128 km $\times$ 128 km) domain. The relatively small size (21.2 km^2) of the study watershed in relation to the size of the atmospheric model domain makes it possible to simulate a large number of rainfall/runoff events with considerably different storm

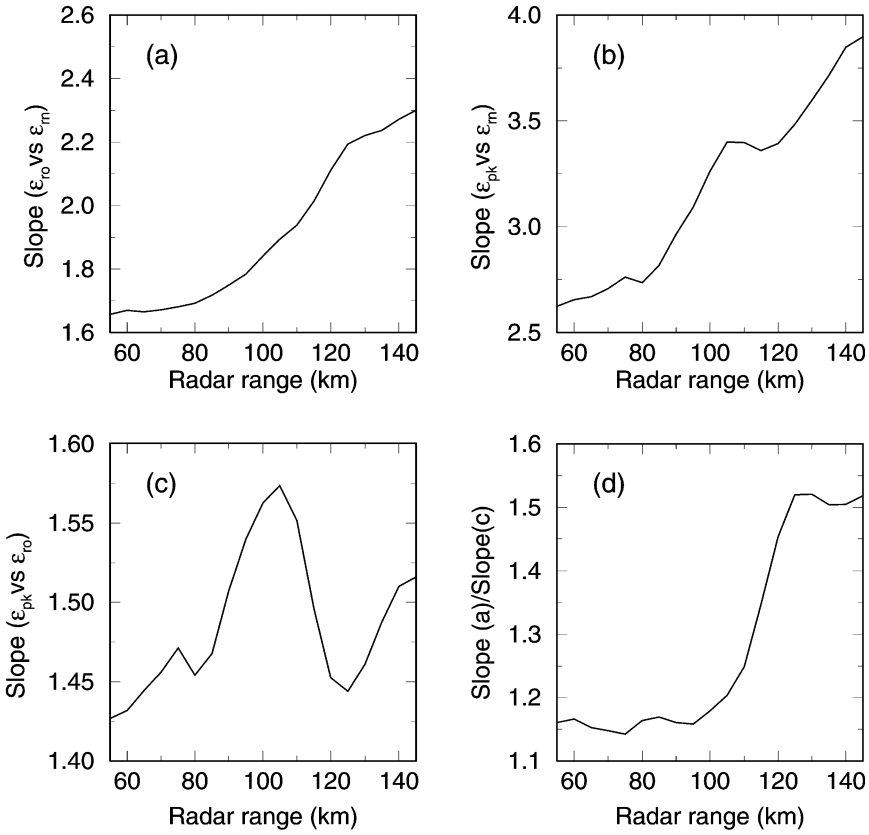

FIG. 6. Range dependence of the relationship between (a) rainfall and runoff errors, (b) rainfall and peak discharge errors, (c) runoff and peak discharge errors, and (d) the ratio of the slopes shown in (a) and (c). See text for details.

morphologies. The high degree of variability within the storm domain allows us to treat the precipitation fields observed at different locations as indicative of midlatitude mesoscale convective complexes of the type that frequently cause flooding in urban areas. We use a two-dimensional, physics-based hydrologic model that was rigorously calibrated using data from a well-monitored experimental watershed. The use of a calibrated and verified physically based model reduces the impact of hydrologic model formulation errors on our results. The radar simulator used is adequate for simulating the errors addressed in this study and the simulated storm serves as an appropriate example of convective storms, at least for the purpose of modeling studies. Although the methodology makes it possible to incorporate many other systematic and random errors associated with radar rainfall estimation process, this study focuses on radar rainfall range-dependent errors. Our choice of the simulation framework allowed us to focus on the statistical properties of the radar rainfall errors and their propagation, rather than on the uncertainty associated with the modeling tools. However, the findings of this study may be dependent on the shape and size of the watershed because we tested only one.

Our simulation study reveals that it is generally very difficult to obtain an accurate estimate of rainfall rate and spatial distribution using a single polarization S-band weather radar, even if it is assumed that the radar is error free, at ranges beyond about 80 km. At ranges less than about 80 km, single-polarization radar rainfall estimates can be fairly accurate. However, other simulation and data-based hydrologic studies should be conducted to verify this conclusion.

Frequency analysis of radar rainfall errors reveals useful information about the statistical distributions of these errors and their propagation through the hydrologic model. The inferred statistical distributions shown in Figs. 3, 4, and 5, are indicative only of the storm analyzed in this experiment. Actual distributions using real data will most certainly be significantly different. We expect that errors will be larger when using real radar data, and that the mean values of errors will be significantly different than 1.0, especially at far ($>$100 km) radar ranges because of the litany of error sources not considered in our study. In effect, our study results represent a ''best-case'' scenario with a perfectly calibrated radar, no hail contamination, no anomalous propagation of the radar beam, no extreme variations from the assumed raindrop-size distribution, and no bright-band effect.

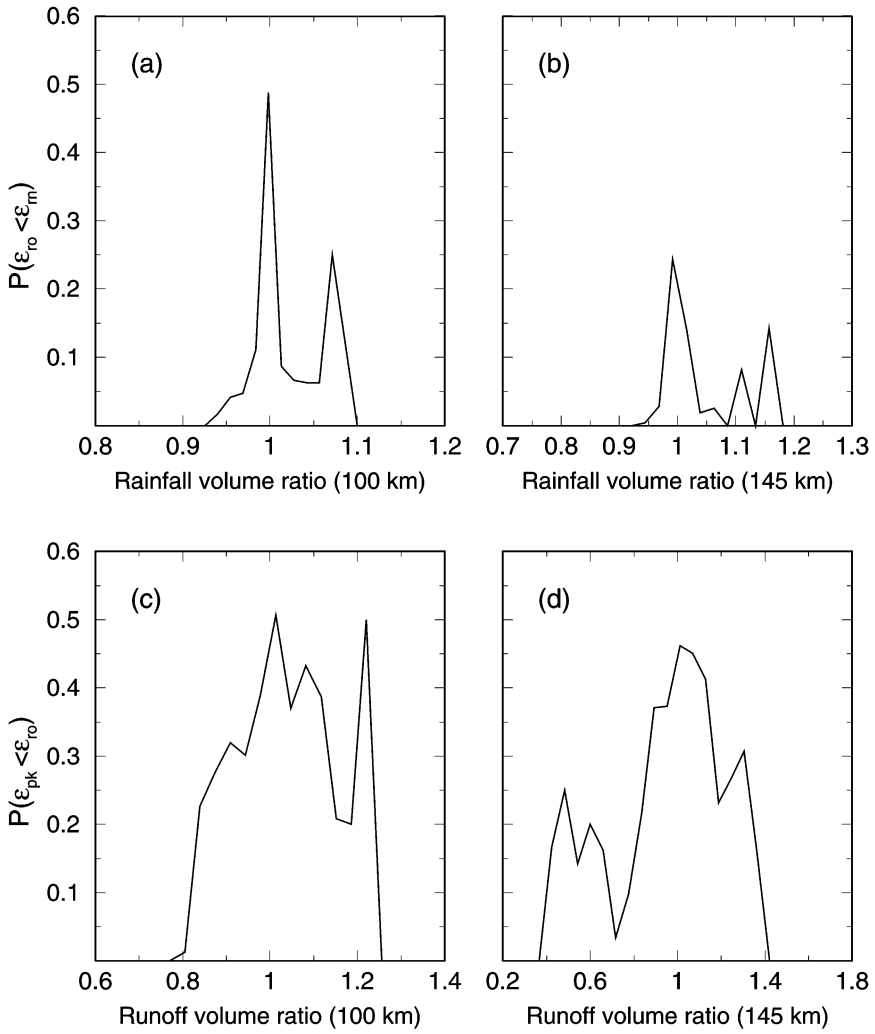

FIG. 7. Probability of (a) radar-estimated runoff volume error (ε_{ro}) not exceeding rainfall volume error (ε_m) and (c) probability of peak discharge error (ε_{pk}) not exceeding runoff volume error (ε_{ro}) for the radar range of 100 km. (b), (d) The same as in left column except radar range of 145 km.

This experiment reveals that radar rainfall estimation errors (expressed as a percentage) are typically amplified in Hortonian runoff predictions as measured by both the predicted runoff volume or peak discharge. Generally, peak discharge errors were always larger than runoff volume errors, and both were larger than rainfall volume errors. Radar rainfall errors and the corresponding runoff errors increase and show higher variance with radar range. Rainfall volume errors and hydrograph errors are generally higher for smaller rainfall events. Amplification of rainfall error increases sharply with radar range, that is, runoff volume and peak discharge errors increase with radar range at a faster rate than rainfall errors.

The uncertainties of hydrologic applications of weather radar are quantified in the form of probability densities. The statistical distribution of a radar-based hydrologic variable for a given ''true'' value of the variable can be very useful in modeling studies and has potential for practical applications. While there are limitations of this study, the methodology can be extended for more rigorous radar data error studies. For example, rainfall and runoff errors were treated at the watershed scale when choosing a finer spatial scale might have been more appropriate in many situations, especially for watersheds of larger sizes. The uncertainty associated with the modeling tools can also be integrated in the total uncertainty, which was not included in this study. Even quality-controlled radar-precipitation observations might contain errors that are larger than those addressed in this study. In spite of the aforementioned limitations, the utility of the methodology of this study and its potential for practical application is important to future studies that will aid in understanding the uncertainties associate with the hydrologic application of weather radar. As well, these features will no doubt prove useful

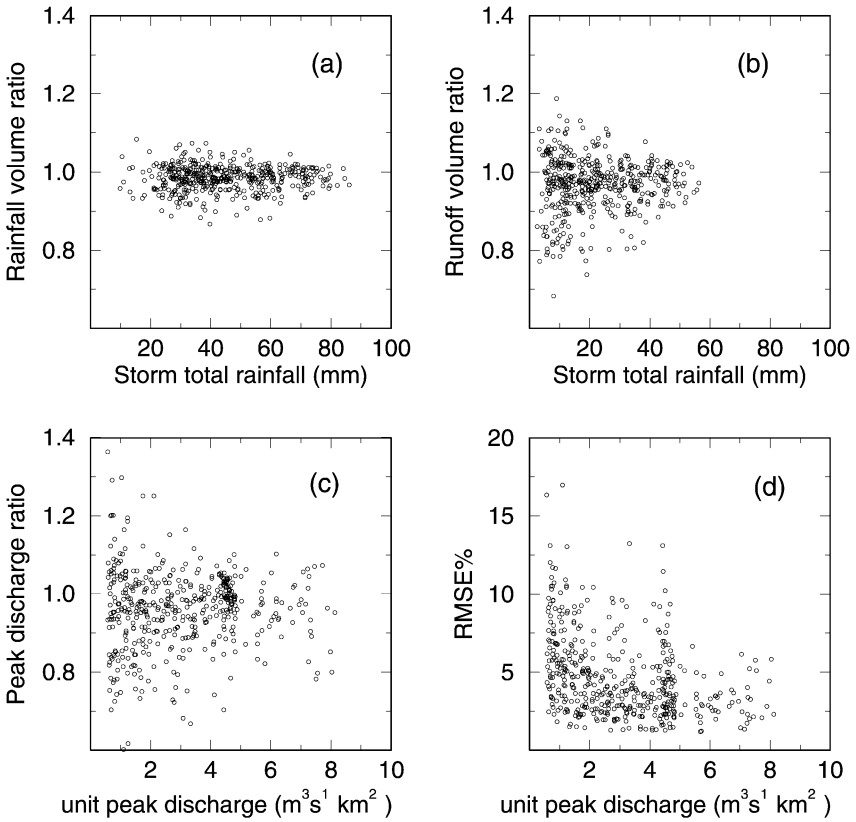

FIG. 8. Relationship between the magnitude of the hydrologic variable and the error in its radar estimate for (a) rainfall volume, (b) runoff volume, (c) peak discharge, and (d) RMSE%. Plots show data for the radar range of 145 km.

in making operational decisions based on radar products.

It is difficult to make accurate corrections for range-dependent errors because the vertical profile of reflectivity is not constant within a storm (e.g., Vignal and Krajewski 2001). This is also true in real-world applications, particularly given the unsteady nature of the reflectivity–rainfall relationship. The use of a hydrologic model to convert uncertain precipitation estimates into runoff predictions creates additional uncertainty. A realistic approach may be to compute the statistics of the relationship between true hydrologic variables and those predicted using radar data and construct probability densities that relate the true and estimated hydrologic variables. Information from all events for which acceptable radar estimates and actual measurements exist can be used to build density functions. Many sources of error are associated with radar rainfall estimation, which makes it reasonable to express information from radar estimates in the form of probabilistic distributions.

Acknowledgments. The U.S. Army Research Office, Mechanical and Engineering Sciences Division, Terrestrial Science Program funded this research, under Grants DAAH04-96-1-0026 and DAAD19-01-1-0629 to the second author. M. Xue was supported by NSF Grants ATM9909007, ATM-0129892 and an FAA grant through NOAA, NA17RJ1227. W. Krajewski was supported by the Rose and Joseph Summers Professorship.

REFERENCES

Alonso, C. V., 1996: Hydrologic research on the USDA Goodwin Creek experimental watershed, northern Mississippi. *Proc. 16th Annual AGU Hydrology Days Conf.,* Fort Collins, CO, Amer. Geophys. Union, 23–36.

Anagnostou, E. N., and W. F. Krajewski, 1997: Simulation of radar reflectivity fields: Algorithm formulation and evaluation. *Water Resour. Res.,* **33,** 1419–1429.

Bingner, R. L., 1996: Runoff simulated from Goodwin Creek watershed using SWAT. *Trans. ASAE,* **39,** 85–90.

Borga, M., E. N. Anagnostou, and W. F. Krajewski, 1997: A simulation approach for validation of a brightband correction method. *J. Appl. Meteor.,* **36,** 1507–1518.

——, ——, and E. Frank, 2000: On the use of real-time radar rainfall estimates for flood prediction in mountainous basins. *J. Geophys. Res.,* **105** (D2), 2269–2280.

Brazil, L. E., 1988: Multilevel calibration strategy for complex hydrologic models. Ph.D. dissertation, Colorado State University, 192 pp.

Chandrasekar, V., and V. N. Bringi, 1987: Simulation of radar reflectivity and surface measurements of rainfall. *J. Atmos. Oceanic Technol.,* **4,** 464–478.

——, and ——, 1988a: Error structure of multiparameter radar and surface measurement of rainfall. Part I: Differential reflectivity. *J. Atmos. Oceanic Technol.,* **5,** 783–795.

——, and ——, 1988b: Error structure of multiparameter radar and surface measurement of rainfall. Part II: X-band attenuation. *J. Atmos. Oceanic Technol.*, **5,** 796–802.

——, ——, N. Balakrishnan, and D. S. Zrnić, 1990: Error structure of multiparameter radar and surface measurement of rainfall. Part III: Specific differential phase. *J. Atmos. Oceanic Technol.*, **7,** 621–629.

Collier, C. G., and J. M. Knowles, 1986: Accuracy of rainfall estimates by radar. III: Application for short-term flood forecasting. *J. Hydrol.*, **83,** 237–249.

Doviak, R. J., and D. S. Zrnic, 1993: *Doppler Radar and Weather Observations.* Academic Press, 562 pp.

Downer, C. W., and F. L. Ogden, 2003: Appropriate vertical discretization of Richards' equation for two-dimensional watershed-scale modeling. *Hydrol. Processes*, in press.

Droegemeier, K. K., and Coauthors, 2000: Hydrological aspect of weather prediction and flood warnings: Report of the Ninth Prospectus Development Team of the U.S. Weather Research Program. *Bull. Amer. Meteor. Soc.*, **81,** 2665–2680.

Fulton, R. A., J. P. Breidenbach, D.-J. Seo, and D. A. Miller, 1998: WSR-88D rainfall algorithm. *Wea. Forecasting*, **13,** 377–395.

Giannoni, F., J. A. Smith, Y. Zhang, and G. Roth, 2003: Hydrologic modeling of extreme floods using radar rainfall estimates. *Adv. Water Resour.*, **26,** 195–203.

Kitchen, M., and P. M. Jackson, 1993: Weather radar performance at long range—Simulated and observed. *J. Appl. Meteor.*, **32,** 975–985.

Krajewski, W. F., and K. P. Georgakakos, 1985: Synthesis of radar-rainfall data. *Water Resour. Res.*, **21,** 764–768.

——, and J. A. Smith, 2002: Radar hydrology: Rainfall estimation. *J. Hydrol.*, **25,** 1387–1394.

——, R. Raghavan, and V. Chandrasekar, 1993: Physically based simulation of radar rainfall data using a space–time rainfall model. *J. Appl. Meteor.*, **32,** 268–283.

Lin, Y.-L., R. D. Farley, and H. D. Orville, 1983: Bulk parameterization of the snow field in a cloud model. *J. Climate Appl. Meteor.*, **22,** 1065–1092.

Ogden, F. L., and P. Y. Julien, 1994: Runoff model sensitivity to radar rainfall resolution. *J. Hydrol.*, **158,** 1–18.

——, and ——, 2002: CASC2D: A two-dimensional, physically-based, Hortonian hydrologic model. *Mathematical Models of Small Watershed Hydrology and Applications*, V. P. Singh and D. K. Frevert, Eds., Water Resources Publications, 69–112.

——, and D. R. Dawdy, 2003: Peak discharge scaling in a small Hortonian watershed. *J. Hydrol. Eng.*, **8,** 64–73.

——, H. O. Sharif, S. U. S. Senarath, J. A. Smith, M. L. Baeck, and J. R. Richardson, 2000: Hydrometeorological analysis of the Fort Collins, Colorado, flash flood of 1997. *J. Hydrol.*, **228,** 82–100.

Pessoa, M. L., R. L. Bras, and E. R. Williams, 1993: Use of weather radar for flood forecasting in the Sieve River basin: A sensitivity analysis. *J. Appl. Meteor.*, **32,** 462–475.

Senarath, S. U. S., F. L. Ogden, C. W. Downer, and H. O. Sharif, 2000: On the calibration and verification of distributed, physically-based, continuous, Hortonian hydrologic models. *Water Resour. Res.*, **36,** 1495–1510.

Shah, S. M. S., P. E. O'Connell, and J. R. M. Hosking, 1996: Modeling the effects of spatial variability in rainfall on catchment response. 2. Experiments with distributed and lumped models. *J. Hydrol.*, **175,** 89–111.

Sharif, H. O., F. L. Ogden, W. F. Krajewski, and M. Xue, 2002: Numerical simulations of radar rainfall error propagation. *Water Resour. Res.*, **38,** 1140, doi:10.1029/2001WR000525.

Tao, W.-K., J. Simpson, and M. McCumber, 1989: An ice-water saturation adjustment. *Mon. Wea. Rev.*, **117,** 231–235.

Ulaby, F. T., R. K. Moore, and A. K. Fung, 1981: *Microwave Remote Sensing Fundamentals and Radiometry.* Vol. 1, *Microwave Remote Sensing: Active and Passive*. Addison-Wesley, 456 pp.

Vignal, B., and W. F. Krajewski, 2001: Large sample evaluation of two methods to correct range-dependent error for WSR-88D rainfall estimates. *J. Hydrometeor.*, **2,** 490–504.

Winchell, M., H. V. Gupta, and S. Sorooshian, 1997: Effects of radar estimated precipitation uncertainty of different runoff generation mechanisms. Tech. Rep. HWR 97-080, Department of Hydrology and Water Resources, The University of Arizona, Tucson, AZ, 285 pp.

——, ——, and ——, 1998: On the simulation of infiltration- and saturation-excess runoff using radar-based rainfall estimates: Effects of algorithm uncertainty and pixel aggregation. *Water Resour. Res.*, **34,** 2655–2670.

Wyss, J., E. R. Williams, and R. L. Bras, 1990: Hydrologic modeling of New England basins using radar rainfall data. *J. Geophys. Res.*, **95** (D3), 2143–2152.

Xue, M., K. K. Droegemeier, V. Wong, A. Shapiro, and K. Brewster, 1995: ARPS version 4.0 user's guide CAPS, 380 pp. [Available from Center for Analysis and Prediction of Storms, University of Oklahoma, Sarkeys Energy Center, Room 1110, 100 East Boyd St., Norman, OK 73019.]

——, ——, and ——, 2000: The Advanced Regional Prediction System (ARPS)—A multiscale nonhydrostatic atmospheric simulation and prediction tool. Part I: Model dynamics and verification. *Meteor. Atmos. Phys.*, **75,** 161–193.

——, and Coauthors, 2001: The Advanced Regional Prediction System (ARPS)—A multiscale nonhydrostatic atmospheric simulation and prediction tool. Part II: Model physics and applications. *Meteor. Atmos. Phys.*, **76,** 143–165.

——, D.-H. Wang, J.-D. Gao, K. Brewster, and K. K. Droegemeier, 2003: The Advanced Regional Prediction System (ARPS), storm-scale numerical weather prediction and data assimilation. *Meteor. Atmos. Phys.*, **82,** 139–170.